Sensitivity Study of a Proposed Polarimetry Diagnostic on ASDEX Upgrade

H. P. Callaghan* and P. J. Mc Carthy*

IPP 5/60

Sept 1994

MAX-PLANCK-INSTITUT FÜR PLASMAPHYSIK

85748 GARCHING BEI MÜNCHEN

MAX-PLANCK-INSTITUT FÜR PLASMAPHYSIK

GARCHING BEI MÜNCHEN

Sensitivity Study of a Proposed Polarimetry Diagnostic on ASDEX Upgrade

H. P. Callaghan* and P. J. Mc Carthy*

IPP 5/60 Sept 1994

*Department of Physics, University College, Cork, Ireland

Die nachstehende Arbeit wurde im Rahmen des Vertrages zwischen dem Max-Planck-Institut für Plasmaphysik und der Europäischen Atomgemeinschaft über die Zusammenarbeit auf dem Gebiete der Plasmaphysik durchgeführt.

Abstract

ASDEX-Upgrade currently uses FIR interferometry (DCN, 195μm) as a technique for measuring line integrated electron density along eight chords of the plasma cross-section. A polarimetry diagnostic based on Faraday rotation using the existing setup would yield $\int n_e \mathbf{B} \cdot \mathbf{dl}$ along the same chords which, in combination with the $\int n_e dl$ measurements, would provide additional information about the poloidal magnetic field. This would be helpful for reconstructing the $q(\psi)$ profile, which is difficult to recover from external magnetic measurements alone.

A sensitivity study to determine the effectiveness of adding polarimetry to ASDEX Upgrade is carried out using function parameterization on a simulated equilibrium database, together with a database of randomly chosen density profiles with four degrees of freedom. The robustness of the recovery in the presence of measurement noise and the effects of plasma birefringence are taken into account.

Contents

1 Introduction

The poloidal magnetic field profile, or equivalently the current density or safety factor profile, is a fundamental quantity of interest in tokamak experiments. One important method of measuring this is based on the Faraday rotation experienced by far infra-red beams of radiation traversing the plasma [1]. On ASDEX-Upgrade, there exists the possibility of adding such a polarimetry diagnostic to the existing FIR interferometry setup. A sensitivity study of the diagnostic is carried out using function parameterization on a database of simulated experimental states, focussing on the recovery of the radial position of inner q surfaces using the external magnetic measurements and the additional polarimetry data.

The general methods of function parameterization and principal component analysis which form the basis of the study are described in the coming sections, as are the principles of polarimetry measurements and the associated effects of plasma birefringence. The recovery of the radial position of the q surfaces of interest is then carried out both with and without the simulated polarimetry signals, and the robustness of the signals in the presence of measurement noise is investigated. In addition, the recovery of the poloidal β and the internal inductance of the plasma l_i (which are related to the current density profile), and q_{axis}, the q value at the magnetic axis, is looked at.

2 Function parameterization

The method of function parameterization consists of the numerical determination, by statistical regression on a database of simulated experimental states, of simple functional representations of parameters characterizing the state of a particular physical system, where the arguments of the functions are statistically independent combinations of diagnostic raw measurements of the system whose geometry is fixed. The technique has very close parallels with artificial neural networks (ANN) in that a 'training' procedure is central to both methods. The following is a breakdown of the main stages involved — a more thorough exploration is made in [2].

The initial phase consists of the generation of a database consisting of randomly chosen states of the system simulated by a computer code. The code should contain an accepted physical model of the system (in our case the plasma is assumed to occupy a sequence of ideal MHD equilibrium states) and should include the geometry of the sensors on the experiment so that experimental measurements can be simulated. Care must be taken at this stage to ensure that the database contains enough variety to accurately reflect that observed in the experiment, since the method detects only those tendencies described within the database and cannot in any way improve on the physical model used to compute the simulated states. In our case, simulated plasma equilibria were generated

using a version of the Garching Equilibrium Code [3] using 12 pseudo-randomly varied independent input parameters.

The second phase is concerned with the actual training procedure, where both model selection/optimization and parameter recovery are carried out off-line. In our analysis, the parameters of interest are recovered with low order polynomial models using multilinear least-squares regression on the simulated diagnostic information. The large number of measurements necessitates dimension reduction techniques described later.

The generation of the database and its subsequent analysis are generally very time-consuming, but once performed, the recovery of plasma parameters using experimental data (which is the operation that must be performed many times) requires only the evaluation of the final function - a relatively trivial task that does not require heavy computational power. This gives FP a great advantage over conventional data interpretation methods: as long as the database reflects the physical reality in both diagnostic and parameter information, a wide variety of effects can be encompassed in the same basic algorithm.

3 Principal component analysis

Principal component analysis (p.c.a.) is a statistical technique which is used as a means of dimension reduction and elimination of multicollinearity — it is employed here to narrow down the number of candidate predictors to be used in regressions from a large set of correlated variables to a smaller subset of linearly independent ones. It operates by selecting uncorrelated linear combinations of maximal variance from the original set of variables. For a more detailed explanation see [2].

More specifically, given a data matrix $\mathbf{X}$ with n observations of p experimental variables $X_1 \ldots X_p$ and its corresponding $p \times p$ covariance matrix S (the covariance of X_i and X_j is defined as $< (X_i - \bar{X}_i)(X_j - \bar{X}_j) >= S_{ij}$), the principal component transformation constitutes a rotation of the coordinate axes in p-space such that they lie along the directions defined by the eigenvectors of S.

The real symmetric matrix S is positive semi-definite with p eigenvalues (λ_i^2), corresponding to orthogonal eigenvectors $\boldsymbol{\gamma_i}$. We index the λ_i^2 by eigenvalue magnitude, so we have $\lambda_1^2 \geq \ldots \geq \lambda_p^2 \geq 0$. The $p \times p$ matrix of eigenvectors (Γ) is formed of columns $\boldsymbol{\gamma_1} \ldots \boldsymbol{\gamma_p}$, which are mutually orthogonal.

The principal component transformation is given by the inner product of the set of centred measurement variables with successive eigenvectors of S:

$$\Phi_i = \sum_{j=1}^{p} \gamma_{ji}(X_j - \bar{X}_j).$$

The Φ_i are the principal components (p.c.'s) of $X_1 \ldots X_p$ (also referred to as the transformed measurements); when evaluated for each observation in $\mathbf{X}$ they form the n sets of p principal component *scores* of $X_1 \ldots X_p$.

The effects of the transformation are two-fold: firstly the transformed variables are now uncorrelated (within the database) by virtue of the fact that the eigenvectors of S are orthogonal, and secondly the variance of Φ_i is less than that of the preceding $\Phi_1 \ldots \Phi_{i-1}$. The number of nonzero eigenvalues of S is exactly the number of degrees of freedom in the data, and any $\boldsymbol{\gamma}$ with a zero eigenvalue leads to a Φ with zero variance (a constant of the database) which has no predictive power (but which can be used to derive constraints on the data). This is the property that leads to dimension reduction: if all principal components were included then there would be no reduction, but the assumption underlying statistical regression analysis based on p.c.a. is that the most significant information will be contained in the first few p.c.'s, and that those beyond a chosen cutoff point (N) can be neglected.

There is no universally accepted criterion for determining the cutoff point for the number of p.c.'s to be included in the regression model, but one requirement leading to a lower bound for N is that there be at least as many predictors as there are degrees of freedom in generating the database. In the context of experimental measurements, all with known noise variance σ^2, an upper bound for N is given by $\lambda_N^2 > \sigma^2$, which is nothing other than the requirement of a good signal to noise ratio. The choice of a cutoff point is thus a compromise between model size, information retained and signal to noise ratio.

For our purposes it is more meaningful to work with the *correlation* matrix $\mathbf{R}$, where $R_{ij} = S_{ij}/\delta_i\delta_j$, and δ_i denotes the standard deviation of X_i etc. In particular, the 34 external magnetic measurements used by FP (fig. 2) for determining the plasma geometry are read into 12-bit digitisers which are calibrated such that the full-scale deflection of the data acquisition electronics fits the largest possible signal that can occur. It is thus natural to standardize the measurements to their own spread (i.e., the square root of the variance); in the context of the p.c.a. it merely means that all of the raw measurements receive equal weighting. Also, since the signal noise is roughly a constant number of bits for each digitiser, it is valid to assume a single noise level σ for all of the standardized variables. $\mathbf{R}$ is a particular type of covariance matrix, one whose diagonal elements are all equal to unity, and thus all properties described for S still hold. Note that due to the standardization of the measurements, trace(S) = sum of the variances of $X_1 \ldots X_p$, whereas trace($\mathbf{R}$) $= p$.

Finally, the transformed measurements are very difficult to assign a physical meaning to — they are, after all, linear combinations of all the original variables which are determined using orthogonality and maximal variance conditions, and this procedure does not lend itself to any simple physical interpretation. Furthermore, it is not always true that maximal variance is the best criterion for selecting the Φ, since it is possible that some Φ may vary widely and yet have little corre-

lation with the response parameter. In such a case, canonical correlation analysis may be a better solution to dimension reduction, since this seeks to identify those linear combinations having the largest correlation with the response parameter.

4 Principles of polarimetry diagnostics

The following is a brief description of the Faraday effect for high-frequency monochromatic e.m. radiation propagating in a plasma with an arbitrary magnetic field $\mathbf{B}$ (the medium is not assumed to be homogeneous), borrowed largely from De Marco and Segre 1972 [1].

The state of polarization of high-frequency monochromatic electromagnetic radiation of wavelength λ changes during propagation in a plasma immersed in a magnetic field. The ray can be generally regarded as the superposition of two characteristic waves (of orthogonal polarizations) whose polarizations remain constant during transit and each of which experiences a slightly different index of refraction. This leads to a phase difference between the two waves which, if the initial ray is plane polarized, manifests itself as a rotation of the plane of polarization of the ray (Faraday rotation).

For linearly polarized radiation, if plasma birefringence effects on the beam due to the component of the field perpendicular to the path is negligible (which is discussed below) and the deflection of the beam due to the changing refractive index does not disturb the trajectory, then the angle of rotation ψ is given by

$$\psi \approx \frac{e}{2m_e c\, n_{e,\mathrm{crit}}(\omega)} \int n_e \mathbf{B} \cdot \mathbf{dl}$$

$$\Rightarrow \quad \psi = 2.6 \times 10^{-13} \ \lambda^2 \int n_e B_{||} dl$$

with ψ in radians, λ in m, $\mathbf{B}$ in T and n_e in m^{-2}.

Thus if ψ is measured along many chords of the plasma and the line integrated electron density $\int n_e dl$ is also known (e.g. from interferometry techniques), then the magnetic field component parallel to the line of sight ($B_{||}$) can be decoupled by FP and its poloidal behaviour determined, yielding information about the toroidal current density (J_t) and thus q.

5 Effects of plasma birefringence

In general, the radiation suffers not only Faraday rotation, but also an ellipticization due to the transverse magnetic field (Cotton-Mouton effect). This has recently been investigated by Segre [5], from whose analysis the following summary has been compiled.

Figure 1:

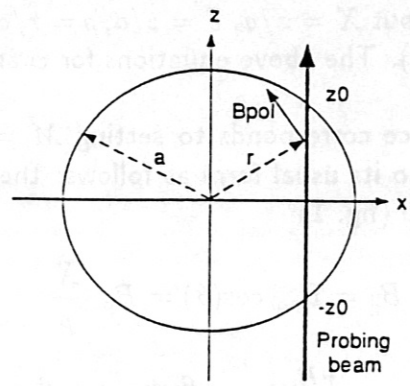

Following Segre's notation, ψ is the Faraday rotation angle and $\tan(\chi)$ is the ellipticity of the final polarization on traversing the plasma — the quantity measured by most polarimeters used to date on tokamaks is $s = \psi + \chi$. For initial $\psi_0, \chi_0 = 0$ with cylindrical symmetry assumed for the plasma density $n(r)$ and the safety factor $q(r)$ and propagation along a vertical chord (z and x are taken to be vertical and along the torus' major radius respectively as in fig. 1), the final parameters ψ, χ are given by:

$$\psi = PXY_3 - \frac{2a}{R}\frac{M^2Y_2}{(1+Xa/R)^4}$$

$$\chi = (PXY_3 - \frac{2a}{R}\frac{M^2Y_2}{(1+Xa/R)^4})\frac{MY_1}{(1+Xa/R)^2}$$

where

$$Y_1 = \int_0^{Z_0} \frac{n(\rho)}{n_0} dZ$$

$$Y_2 = \int_0^{Z_0} dZ \frac{n(\rho)}{n_0}\frac{Z}{q(\rho)} \int_0^{Z} dZ' \frac{n(\rho')}{n_0}$$

$$Y_3 = \int_0^{Z_0} \frac{n(\rho)}{n_0}\frac{q_a}{q(\rho)} dZ$$

are form factors of order unity,

$$P = 10.4\lambda^2 n_0 I_p$$

$$M = 2.42\lambda^3 B_0^2 n_0 a$$

are dimensionless quantities, and λ(mm) is the radiation wavelength, $n_0(10^{20}\mathrm{m}^{-3})$ is the central plasma density, I_p(MA) is the plasma current, B_0(T) is the toroidal magnetic field at $r = 0$ and a and R are the tokamak major and minor radii respectively (m). Propagation is in the z direction on a chord a distance x from the plasma centre and we put $X = x/a, Z = z/a, \rho = r/a = (X^2+Z^2)^{1/2}, Z_0 = (1-X^2)^{1/2}, q_a = q(\rho = 1)$. The above equations for ψ and χ are valid for small M, P and for small X.

Neglect of birefringence corresponds to setting $M = 0$, in which case the expression for ψ reduces to its usual form as follows: the parallel component of the poloidal magnetic field (fig. 1)

$$B_{\|} = B_{\mathrm{pol}}\cos(\theta) = B_{\mathrm{pol}}\frac{X}{\rho}$$

$$\text{Now} \qquad q(r) = \frac{rB_{\mathrm{tor}}}{RB_{\mathrm{pol}}} \Rightarrow \frac{q_{\mathrm{axis}}}{q(r)} = \frac{a}{B_{\mathrm{pol}}(a)}\frac{B_{\mathrm{pol}}(r)}{r}$$

$$\text{and} \qquad B_{\mathrm{pol}}(a) = \frac{\mu_0 I}{2\pi a} = \text{const.}$$

$$\text{Thus} \qquad \frac{q_{\mathrm{axis}}}{q(r)} = \frac{2\pi a^2}{\mu_0 I}\frac{B_{\mathrm{pol}}(r)}{r} = \frac{2\pi a}{\mu_0 I}\frac{B_{\mathrm{pol}}(r)}{\rho}$$

$$Y_3 = \frac{2\pi a}{\mu_0 I}\int_0^{Z_0}\frac{n(\rho)}{n_0}\frac{B_{\mathrm{pol}}(\rho)}{\rho}dZ.$$

$$a\,dZ = dz \qquad \text{and} \qquad \frac{B_{\mathrm{pol}}(\rho)}{\rho} = \frac{B_{\|}}{X}$$

$$\Rightarrow Y_3 = \frac{2\pi a}{\mu_0 I}\int_0^{z_0}\frac{n(\rho)}{n_0}\frac{B_{\|}}{X}dz.$$

$$\text{Finally} \qquad \psi = PXY_3 = 10.4\lambda^2\frac{2\pi}{\mu_0}\left(\frac{1}{2}\int_{-z_0}^{z_0} nB_{\|}dz\right) = 2.6\times10^{-13}\lambda^2\int_{-z_0}^{z_0} nB_{\|}dz,$$

where all quantities in the final formula are in SI units once again.

In the case of modest electron densities and magnetic fields, it can be arranged by suitable choice of input polarization that $\psi \gg \chi$, and Faraday rotation dominates the signal s [5] given by:

$$s(X) = \psi + \chi = \left(PXY_3 - \frac{2a}{R}\frac{M^2Y_2}{(1+Xa/R)^4}\right)\left(1 + \frac{MY_1}{(1+Xa/R)^2}\right)$$

In the more extreme regimes of a tokamak such as AUG it is of interest to look for an upper bound on the form factors $Y1, Y2, Y3$ and hence estimate the overall effect of birefringence on s.

Assuming that the density profile is of the form $n_{e(\rho)} = n_{\rho=0}(1-\rho^2)$, $q_{\mathrm{axis}} \geq 1$ and $q_a \leq 6$ then upper bounds for $Y1, Y2, Y3$ follow easily:

$$Y_1 \leq \tfrac{2}{3}$$
$$Y_2 \leq \tfrac{1}{3}$$
$$Y_3 \leq 4$$

Thus the relative importance of birefringence compared to Faraday rotation can be estimated.

The usual method of interpretation of the polarimetry data for circular plasmas is Abel inversion of the line integrals — this allows the reconstruction of $B_{\|}$ in terms of the polarimeter signal s. For such a procedure however, the ellipticity acquired by the beam due to the perpendicular component of the magnetic field is highly undesirable since $s = \psi + \chi$ then no longer measures simply Faraday rotation: a significant χ leads to an error in s which must be taken into account, and even if χ is small, non-negligible birefringence distorts the Faraday angle ψ itself as detailed above.

The simulated polarimetry data (see later) in the FP database are, at present, purely proportional to ψ and assume zero ellipticization of the beam. On the surface, this would appear to present a problem: the database does not account for the Cotton-Mouton effect and the results, which we present later, could therefore be judged to be optimistic. However, since q and $n_e(\rho)$ are known in the database it is possible to accurately account for the birefringence effects by numerical integration of Y_1–Y_3 and inclusion of this contribution in the simulated polarimetry data. So as far as FP is concerned, this is a known contribution to the evolution of the polarization state and can thus be included in the generation of the database, and there are no difficulties with the full treatment apart from the more involved off-line calculation of the simulated measurements. Otherwise the entire procedure remains the same: the model is simply optimised (or in the language of artificial neural networks, *trained*) on the new measurements. This is one of the most attractive features of FP and ANN over conventional interpretation methods: as long as the predictors can be programmed to accurately reflect the physical reality, then any complicated side-effects are automatically accounted for in the final optimised function and require no additional analysis.

6 Database details

The database used in analysis is a subset of the ASDEX Upgrade equilibrium database used for FP and contains approximately 800 lower single null plasmas of area greater than $0.9\mathrm{m}^2$. This excludes $\sim$ 40 % of all category 4 plasmas, but the excluded equilibria differ strongly from the standard configuration. All profiles have been scaled to correspond to a plasma current I_p of 1MA and a magnetic field of 2.5T at $R = 1.65$m. Fig. 4 shows a few of the more extreme examples that are still included in the database used here.

The toroidal current density profile, which is central to the present work, is

Figure 2: Magnetic diagnostics on AUG: the 34 measurements which FP uses to determine the geometry of the plasma

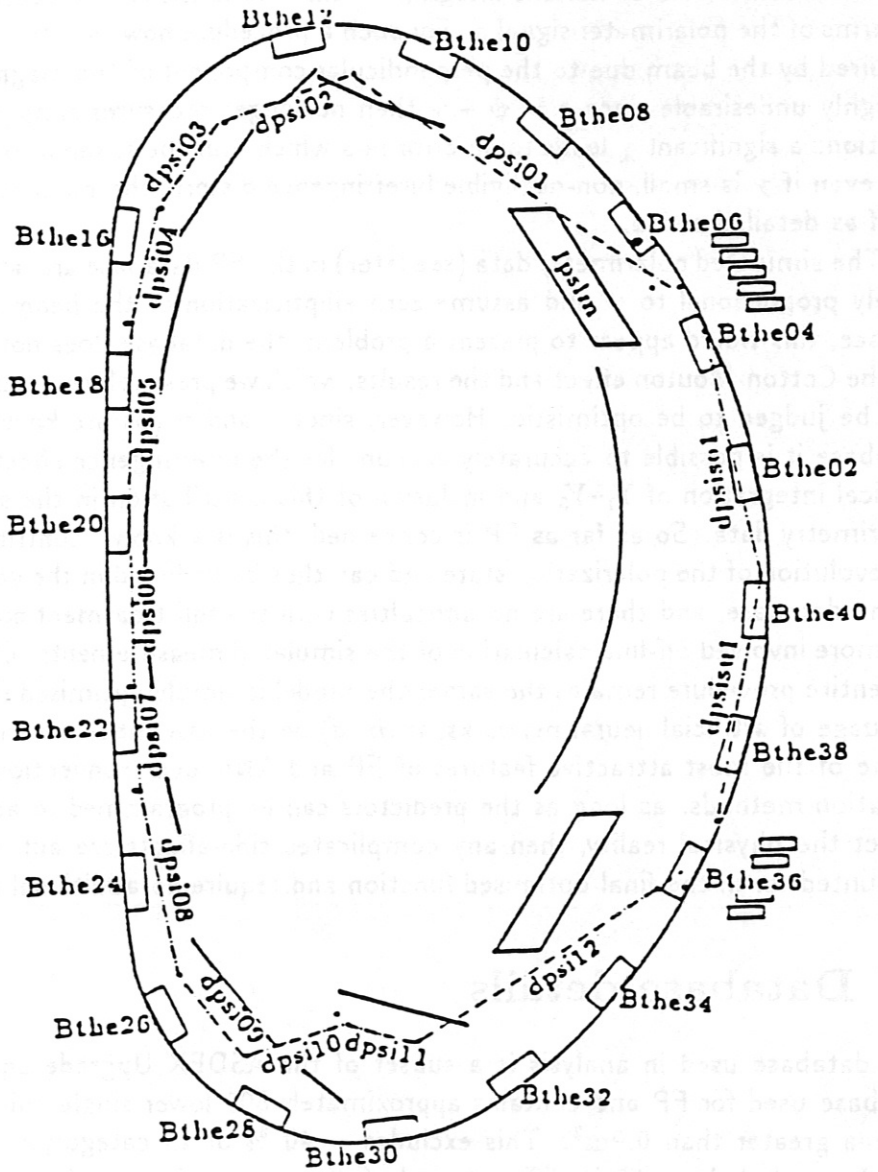

Figure 3: Existing interferometry setup on AUG: 8 FIR channels (DCN, 195μm)

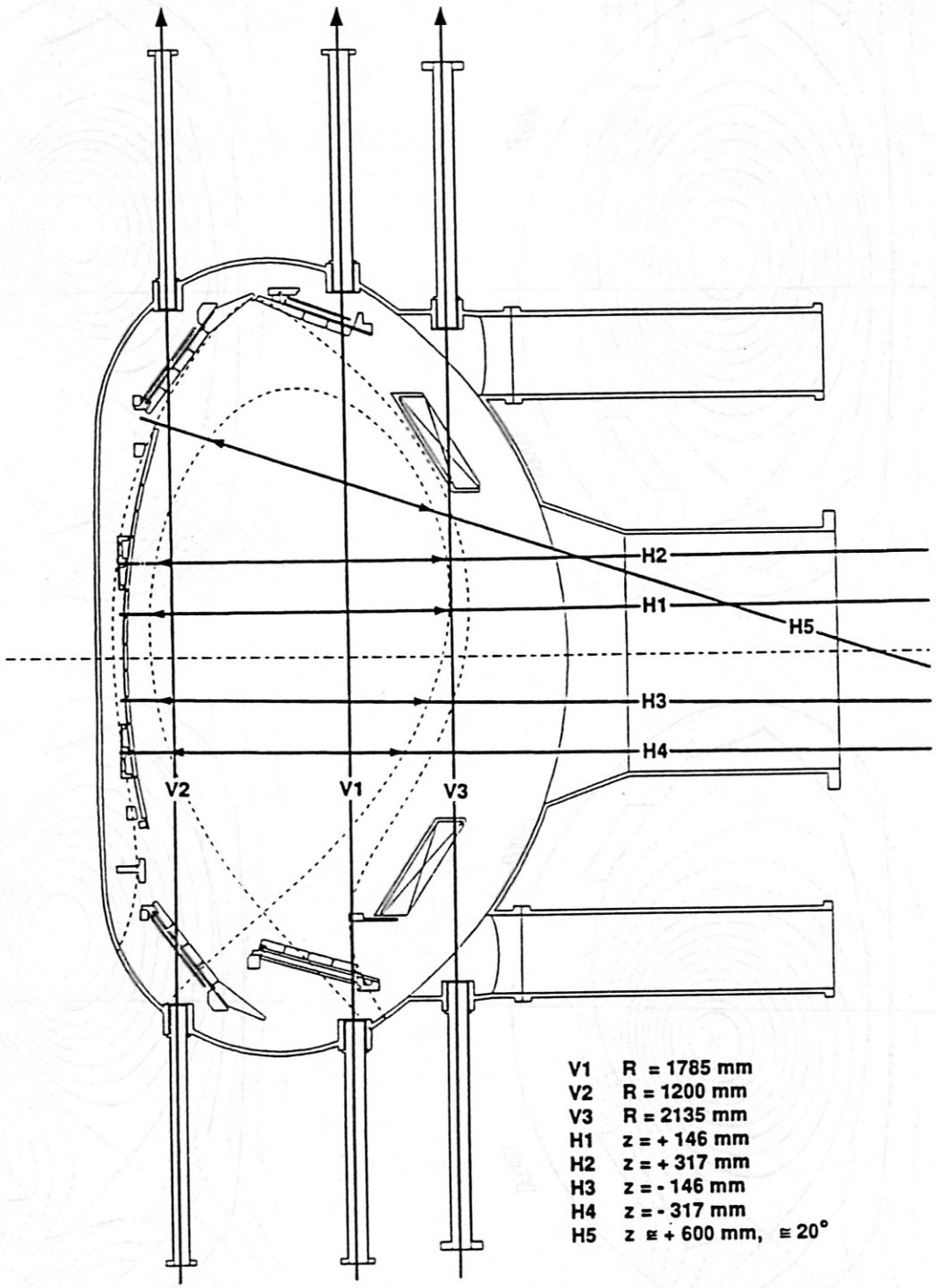

Figure 4: Examples of equilibria in the database

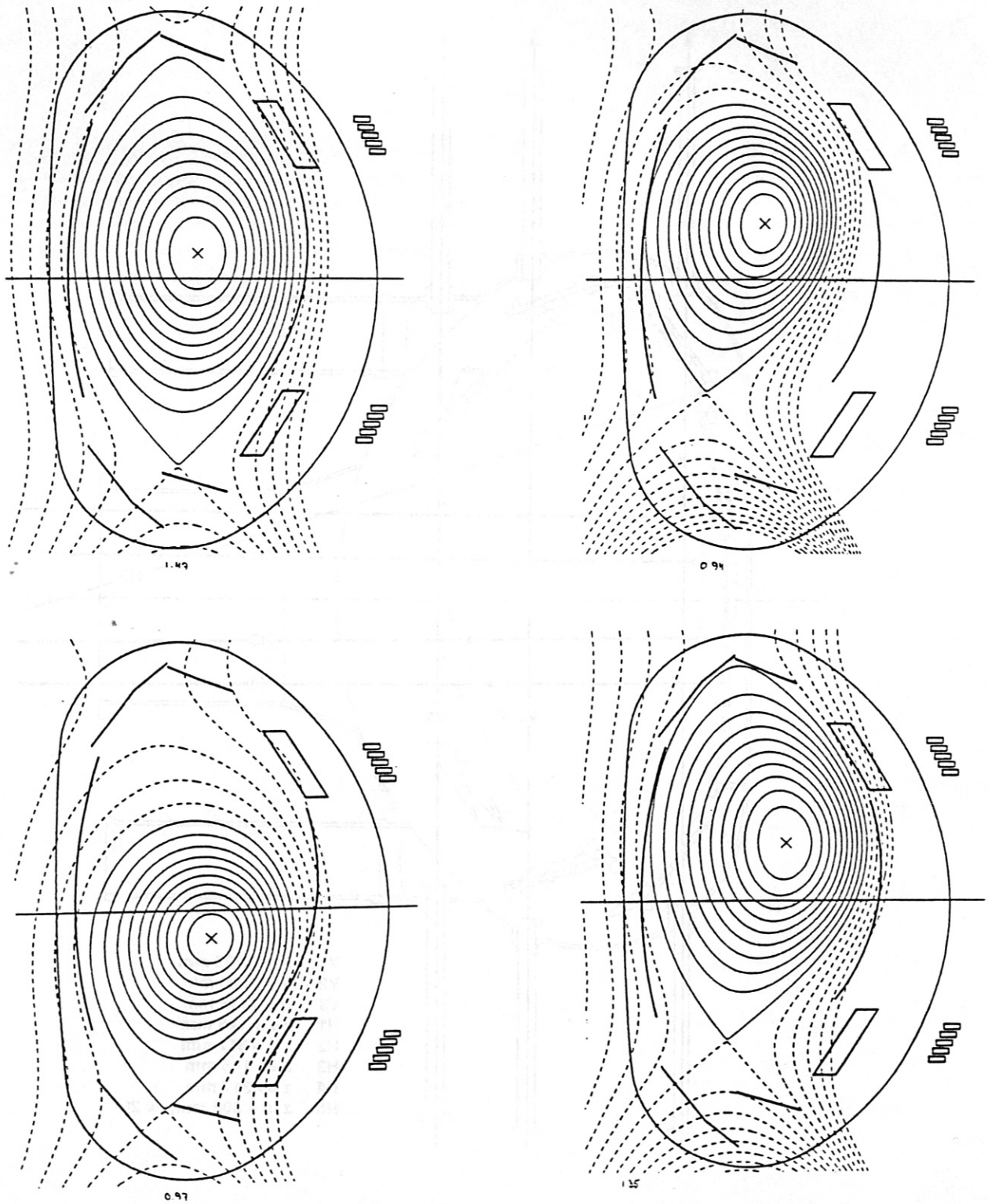

parameterized in the equilibrium code as

$$j_t = C_{p'}\hat{\psi}^{LL_{p'}}\, R + C_{FF'}\hat{\psi}^{LL_{FF'}}/R$$

Here, $\hat{\psi} = \frac{(\psi-\psi_b)}{(\psi_a-\psi_b)}$ where ψ is the poloidal stream function and the subscripts 'a' and 'b' refer to the values it takes at the magnetic axis and plasma boundary, respectively. The right-hand side arises from the following parameterization of the two free flux functions in the Grad-Shafranov equation:

$$p'(\psi) = C_{p'}\hat{\psi}^{LL_{p'}}; \qquad \frac{FF'(\psi)}{\mu_o} = C_{FF'}\hat{\psi}^{LL_{FF'}}$$

Thus $LL_{p'}$ and $LL_{FF'}$ are shape parameters for the (derivative) pressure and poloidal current profiles. $C_{p'}$ and $C_{FF'}$ are related to β_{pol} and $1-\beta_{pol}$, respectively. For a fuller description see [2].

In addition to the information normally stored in the database, each equilibrium was assigned an electron density (n_e) profile parameterized as:

$$n_{e(\mathrm{plasma})} = a + b\rho_\psi^2 + c\rho_\psi^4 + d\rho_\psi^6,$$

where ρ_ψ is the normalised flux surface radius and the set of coefficients a, b, c, d are chosen randomly from a database of 2000 experimental profile fits to electron density and temperature measurements from the ASDEX Thomson scattering diagnostic. In the scrape-off layer a fifth parameter (the fall-off length λ) was added:

$$n_{e(\mathrm{sol})} = n_{e(\mathrm{boundary})}\mathrm{e}^{-\mathrm{x}_\psi/\lambda}$$

where 1cm$\leq \lambda \leq$ 3cm and x_ψ is the distance along the major radius in the $z = z_{geo}$ plane from the plasma boundary to the vacuum flux surface ψ.

Using the n_e profile assigned to each equilibrium and the description of $\mathbf{B}$ from the equilibrium database, the line integrals $\int n_e dl$ (simulating existing interferometry data) and $\int n_e \mathbf{B}\cdot\mathbf{dl}$ (simulating the new polarimetry data) along the 8 DCN chords (see fig. 3) were numerically computed for both the plasma and scrape-off layer regions separately. These new predictors were added to the magnetic measurements in models for FP regressions.

The scrape-off layer contribution to the line integrals is important for the recovery, in that it provides zeroth order continuity in n_e at the boundary. In many cases the line of sight for one or more channels does not cut the plasma boundary, resulting in a zero plasma contribution to the corresponding line integrals. This poses problems for the regression since a zero $\int n_e dl$ or $\int n_e \mathbf{B}\cdot\mathbf{dl}$ provides no information regarding how far the plasma is from the given chord. The more realistic *total* line integrals (sum of plasma and s.o.l. contributions) were exclusively used in regressions — these yielded better overall recoveries than the separated contributions and, in any case, only the totals are available from the experiment.

Table 1: Summary statistics for the line integrals

	Signal	H1	H2	H3	H4	H5	V1	V2	V3
Mean	$\int n_e dl$	0.43	0.35	0.36	0.23	0.15	0.56	0.12	0.02
Std	$\int n_e dl$	0.31	0.29	0.28	0.22	0.19	0.42	0.13	0.04
Max	$\int n_e dl$	2.04	1.85	1.86	1.62	1.47	2.62	1.08	0.55
Mean	$\int n_e B_\parallel dl$	1.23	3.27	-3.28	-3.01	2.33	-4.86	2.66	-0.60
Std	$\int n_e B_\parallel dl$	4.44	3.95	3.96	3.29	2.83	5.39	2.97	1.11
Min	$\int n_e B_\parallel dl$	-22.96	-21.26	-23.14	-26.84	-3.25	-41.42	-0.12	-15.07
Max	$\int n_e B_\parallel dl$	21.62	26.65	27.75	20.82	24.38	22.95	27.75	0.00
Mean	$\parallel \int n_e B_\parallel dl \parallel$	3.35	3.85	3.95	3.23	2.34	5.47	2.66	0. 60
Std	$\parallel \int n_e B_\parallel dl \parallel$	3.16	3.39	3.29	3.07	2.83	4.77	2.97	1. 11
Max	$\parallel \int n_e B_\parallel dl \parallel$	22.96	26.65	27.75	26.84	24.38	41.42	27.75	15. 07

Table 1 details the summary statistics for the simulated line integrated density and $\int n_e B_\parallel dl$, with the $\int n_e dl$ in $10^{20}\mathrm{m}^{-2}$ and $\int n_e B_\parallel dl$ in degrees for I_p=1MA.

The line integrated density is reasonable at a few times $10^{19}\mathrm{m}^{-2}$. On average, the Faraday rotation is roughly 3–4° for each of the channels: the anomalous maximum and minumum values of over 20° are due to a very few extreme equilibria in the database and are highly atypical.

7 Model selection

From previous FP work [2], it was found that a quadratic model of the form

$$g(\Phi_1,\ldots,\Phi_N) = a + \underbrace{\sum_{i=1}^{N} b_i\Phi_i}_{\text{linear}} + \underbrace{\sum_{i=1}^{N} c_i\Phi_i^2}_{\text{quadratic}} + \underbrace{\sum_{i=1}^{N}\sum_{j=1}^{i-1} c_{ij}\Phi_i\Phi_j}_{\text{mixed}}$$

was the best compromise between model size and quality of fit for recovery of a plasma parameter g in terms of the significant principal components $\Phi_1 \ldots \Phi_N$. The same basic model is used in the analysis which follows. Higher order models result in a prohibitively large number of fitted parameters and typically do not offer significant improvement in recovery, whilst linear models give an inadequate fit.

Figure 5:

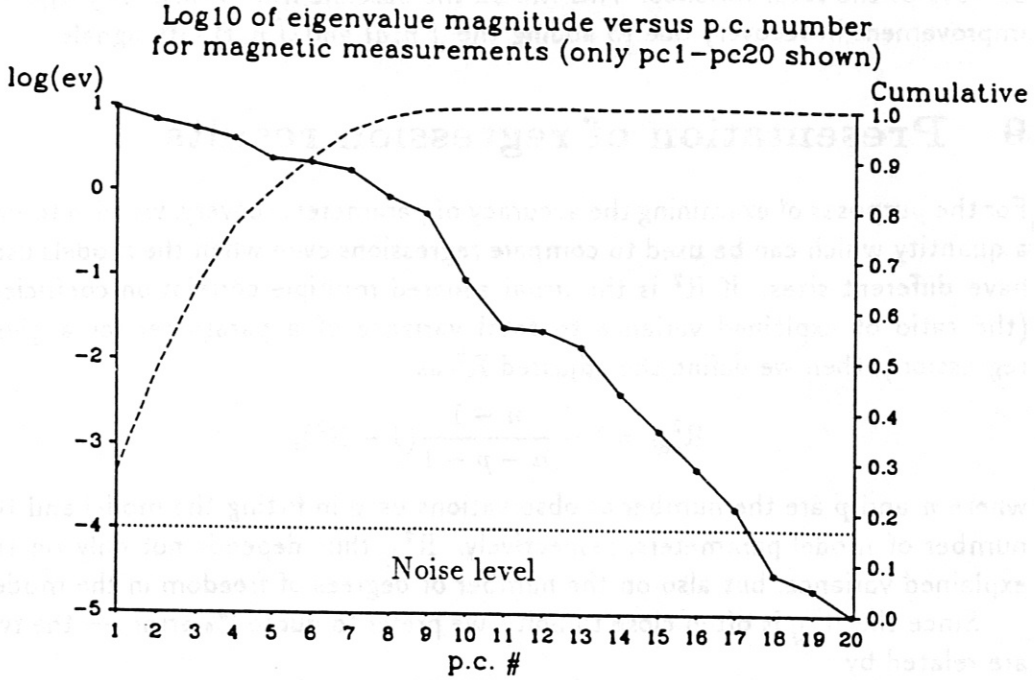

8 Selection of magnetic measurement p.c. cutoff

The 34 magnetic measurements illustrated in fig. 2 represent the set of candidate predictors with which FP determines the geometry of the plasma. Since there are many more measurements then degrees of freedom, a p.c.a. is carried out on this set of variables within the $\sim$ 800 case database in order to eliminate multicollinearity and minimize the number of predictors used (thereby avoiding ill-conditioned regressions and excessively large models).

Fig. 5 shows a log plot of the eigenvalues of the correlation matrix (variances of the transformed measurements Φ_i as explained previously) along with the cumulative fraction of the total variance explained as a function of p.c. number. The assumed noise level in the signals (1%) [2] is marked as a dotted line for clarity, and only the first twenty p.c.'s are included — the rest have negligible eigenvalues.

In selecting the optimum number of p.c.'s to include in regressions we ensure that p.c.'s with a low signal to noise ratio are beyond the cutoff point: these hold little useful information and serve only to needlessy enlarge the model size.

We seek to capture as much variance with as few p.c.'s as possible. The

14^{th} p.c. has an eigenvalue of 0.004, which is equivalent to a signal to noise ratio of 40 at the assumed 1% noise level — choosing the cutoff here we retain 99.99% of the total variance. This will be the baseline from which we judge the improvement in recovery due to adding the $\int n_e dl$ and $\int n_e \mathbf{B} \cdot \mathrm{dl}$ signals.

9 Presentation of regression results

For the purposes of examining the accuracy of parameter recovery, we wish to find a quantity which can be used to compare regressions even when the models used have different sizes. If R^2 is the usual squared multiple correlation coefficient (the ratio of explained variance to total variance of a parameter for a given regression), then we define the adjusted R^2 as

$$\mathrm{R}^2_{\mathrm{adj}} = 1 - \frac{n-1}{n-p-1}(1-\mathrm{R}^2),$$

where n and p are the number of observations used in fitting the model and the number of model parameters, respectively. $\mathrm{R}^2_{\mathrm{adj}}$ thus depends not only on the explained variance, but also on the number of degrees of freedom in the model.

Since the $\mathrm{R}^2_{\mathrm{adj}}$ is often close to unity, we prefer to quote '% error' — the two are related by

$$\%\ \mathrm{error} = \sqrt{1-\mathrm{R}^2_{\mathrm{adj}}} \times 100.$$

In order to obtain an idea of the spatial error in metres, it is necessary to find an approximate relation between ρ_ψ and the geometric radial coordinate ρ_{geo}.

$$\rho_\psi = \text{ normalised } \psi \text{ coordinate} = \frac{\psi_a - \psi}{\psi_a - \psi_b},$$

where ψ_a and ψ_b are the flux values on the magnetic axis and the boundary flux surface, respectively.

$$\text{Defining } \rho_{geo} = \sqrt{\frac{\mathrm{area}(\psi)}{\mathrm{area(plasma)}}}$$

$$\text{we have } \frac{d\rho_{\mathrm{geo}}}{\rho_{\mathrm{geo}}} \approx \frac{1}{2}\frac{d\rho_\psi}{\rho_\psi}$$

since $\rho(\psi) \propto \mathrm{area}(\psi)$ for a circular plasma with constant current density. Assuming this to hold approximately for AUG, we obtain an estimate of the spatial error in the flux surface radius:

$$dr_{\mathrm{geo}} \approx \frac{1}{2}\frac{d\rho_\psi}{\sqrt{\rho_\psi}}a$$

where a is the appropriately weighted minor radius of the plasma. This relation will be sufficient to estimate the spatial error with which the q surfaces are identified.

10 Electron density recovery

As a preliminary exercise, recovery of the density profile was attempted using the magnetic measurements together with the interferometry density line integrals $\int n_e dl$. Note that the line integrals were included noise-free here: the experimental noise level is 2% [6] which is added as a normally distributed pseudo-random error.

In order to avoid the unphysical situation of recovering the density in terms of its square, a slightly different model to that described previously was used, where only mixed second order terms in n_e (i.e. involving a product of a line integral and a magnetic p.c.) were admitted to the regression model. The electron density was generated at $\rho_\psi = 0, 0.1, 0.2, \ldots, 1.0$ and a model consisting of fourteen magnetic measurement p.c.'s and the eight $\int n_e dl$ was chosen to recover n_e. In table 2, columns 2–4 are in $10^{16} m^{-3}$, and the relative error (final column) is the rmse divided by the average value of $n_e(\rho_\psi)$.

Table 2: Recovery of $n_e(10^{16} m^{-3})$ from 14 magnetic p.c.'s (1% noise) and 8 noise free $\int n_e dl$

Variable	Mean	Std. Dev.	RMSE	Adj. R^2	% Error	$\frac{\text{RMSE}}{\text{Mean}}(\%)$
$n_e(0.0)$	8145	5357	105	0.9996	2.0	1.2
$n_e(0.1)$	8000	5224	88	0.9997	1.7	1.1
$n_e(0.2)$	7578	4849	58	0.9999	1.2	0.8
$n_e(0.3)$	6918	4300	85	0.9996	2.0	1.2
$n_e(0.4)$	6083	3665	133	0.9987	3.6	2.2
$n_e(0.5)$	5146	3021	148	0.9976	4.9	2.9
$n_e(0.6)$	4183	2415	117	0.9976	4.9	2.8
$n_e(0.7)$	3260	1882	112	0.9964	6.0	3.4
$n_e(0.8)$	2412	1462	195	0.9822	13.3	8.1
$n_e(0.9)$	1626	1042	210	0.9595	20.1	12.9
$n_e(1.0)$	816	562	195	0.8798	34.7	23.9

The densities are generally well recovered except towards the edge values, which are quite poorly diagnosed beyond the 70% surface. Note that this explicit recovery of the profile is *not* necessary from FP's standpoint for interpreting the $\int n_e \mathbf{B} \cdot \mathbf{dl}$ measurements: it is sufficient to include the $\int n_e dl$ as predictors in the model for $q(\psi)$.

The fluctuations of the RMSE along the profile are most likely the result of the complex dependency of the correlation of the line integrals with the density on both the length of the channel in the plasma and the shape of the n_e profile. The trends revealed in both the % and relative errors are simpler, however, with a minimum at $\rho = 0.2$ and thereafter monotonically increasing towards the edge.

11 Identification of q surfaces

The safety factor q is a flux surface quantity which is important in determining the MHD stability properties of the plasma — since q is derived from an integral of the toroidal current density j_t and is hence linked to the poloidal magnetic field, we expect to improve FP recovery of q by adding the simulated polarimetry measurements to the equilibrium magnetic measurements. Furthermore, the improvement should be more significant towards the centre of the plasma since q is well determined at the boundary by external magnetic data.

To investigate this, the radial position of the surfaces for q=1.25, 1.5, 1.75, and 2.0 were recovered, firstly using the magnetic measurements alone to establish a baseline from which to judge the recovery, and then with the interferometry and polarimetry signals added.

12 Recovery of ρ

Table 3 details the regression results for the radial positions of the q=1.25, 1.5, 1.75, 2.0 surfaces using a quadratic model consisting of the fourteen magnetic p.c.'s which were selected in the last section. The RMSE in mm is obtained from the rough approximation derived earlier.

As expected, the recovery improves as we move from the inner $q = 1.25$ surface towards the outer $q = 2.0$ surface, verifying the fact that the external magnetic measurements are more suited to predicting q nearer the plasma boundary than far inside the plasma. Also the errors in $\rho_{1.5}$ and $\rho_{1.75}$ are not quoted in results from here on, since they more or less linearly interpolate between those of $\rho_{1.25}$ and $\rho_{2.0}$.

From the given baseline of 14 magnetic measurement p.c.'s we add the eight interferometry ($\int n_e dl$) signals and obtain little improvement in recovery — this is as it should be since these carry no information on the poloidal field by themselves. They are, however, correlated with the size of the plasma and thus including them as predictors gives a small $\approx 1\%$ decrease in percentage error for the ρ as shown on table 4.

Table 3: Recovery of ρ with 14 magnetic p.c.'s (1% noise)

Variable	RMSE	Adj. R^2	% Error	RMSE(mm)
$\rho_{1.25}$	0.029	0.9731	16.4	14.8
$\rho_{1.5}$	0.016	0.9839	12.7	7.3
$\rho_{1.75}$	0.009	0.9908	9.6	4.0
$\rho_{2.0}$	0.006	0.9941	7.7	2.4

Table 4: Recovery of ρ with 14 magnetic p.c.'s (1% noise) + 8 $\int n_e dl$ (2% noise)

Variable	RMSE	Adj. R^2	% Error	Error(mm)
$\rho_{1.25}$	0.027	0.9766	15.3	13.8
$\rho_{1.5}$	0.016	0.9858	11.9	6.8
$\rho_{1.75}$	0.009	0.9915	9.2	3.8
$\rho_{2.0}$	0.006	0.9947	7.3	2.3

We now add the $\int n_e \mathbf{B} \cdot \mathrm{dl}$ one by one and plot the recovery error versus number of channels added, to assess the effectiveness of the polarimetry measurements in improving the recovery (fig. 6).

Figure 6:

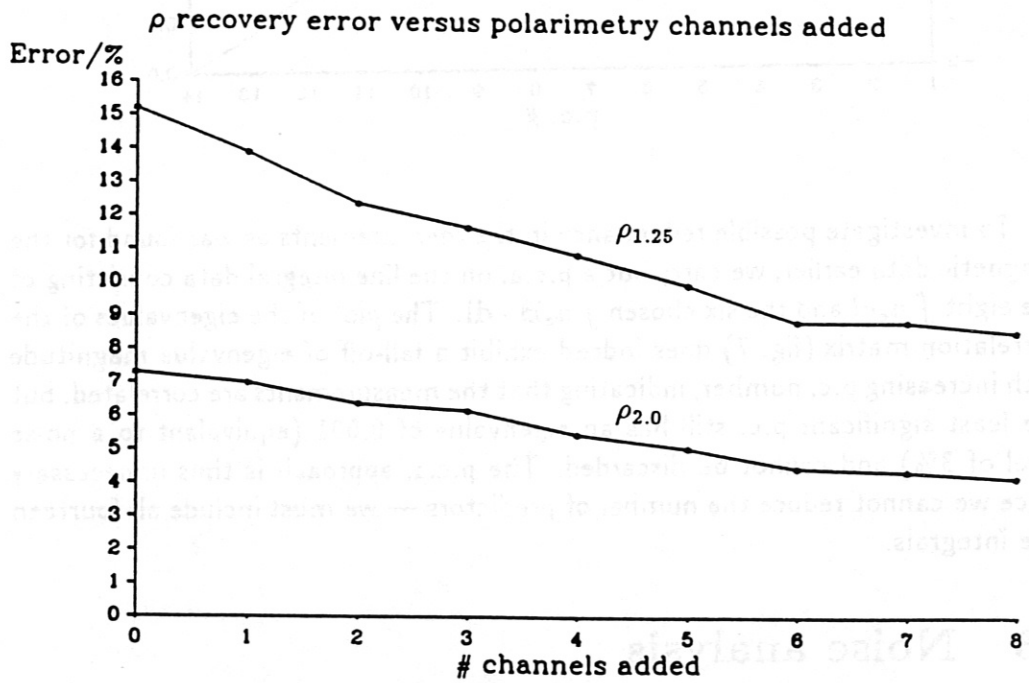

The improvement in recovery is minimal for channels 7 and 8, which correspond to V2 and V3 on fig. 3. These are grazing channels which generally sample the outer portion of the plasma, and whose information is already contained in the external magnetic measurements. This leads us to conclude that only the first six polarimetry signals are of interest in our study — these correspond to channels H1-H5 and V1 on fig. 3.

Figure 7:

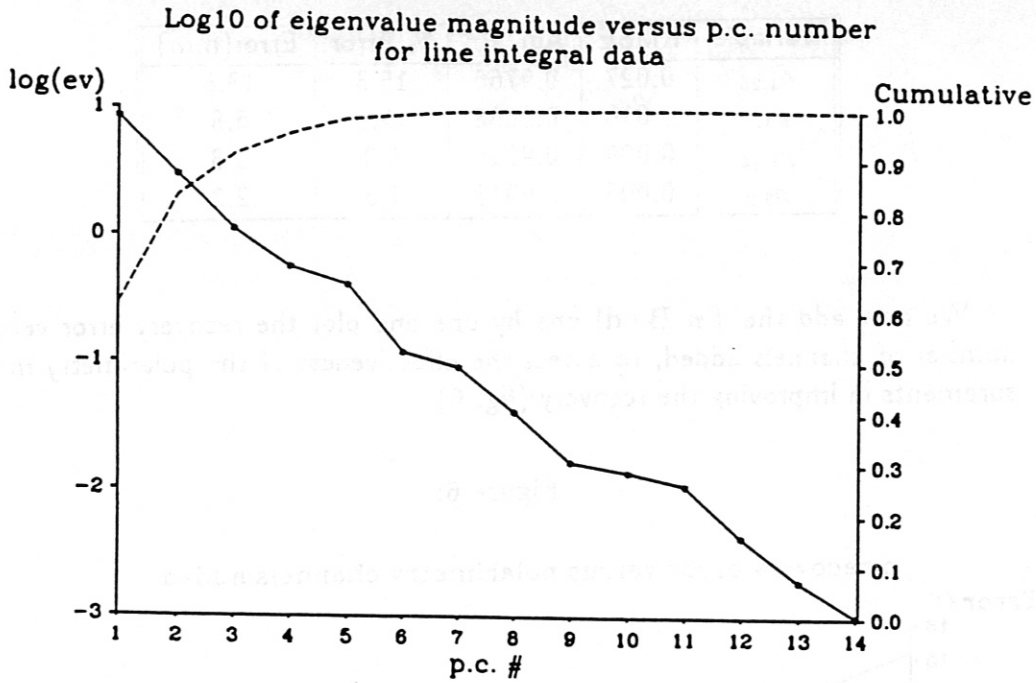

To investigate possible redundancy in the measurements as was found for the magnetic data earlier, we carry out a p.c.a. on the line integral data consisting of the eight $\int n_e dl$ and the six chosen $\int n_e \mathbf{B} \cdot \mathbf{dl}$. The plot of the eigenvalues of the correlation matrix (fig. 7) does indeed exhibit a fall-off of eigenvalue magnitude with increasing p.c. number, indicating that the measurements are correlated, but the least significant p.c. still has an eigenvalue of 0.001 (equivalent to a noise level of 3%) and cannot be discarded. The p.c.a. approach is thus unnecessary since we cannot reduce the number of predictors — we must include all fourteen line integrals.

13 Noise analysis

To examine the sensitivity of the polarimetry measurements in the presence of noise, a series of regressions were performed for a model of fourteen magnetic measurement p.c.'s, eight polarimetry line integrals (with an assumed 2% error [6]) and the six polarimetry signals, for absolute errors of 0.0–1.2°. Note that it is appropriate to add absolute (as opposed to percentage) errors to the polarimetry signals, since in reality the factor limiting the accuracy of the measurement will be the fixed finite maximum resolution of the polarimeter. Fig. 8 details recovery

Figure 8:

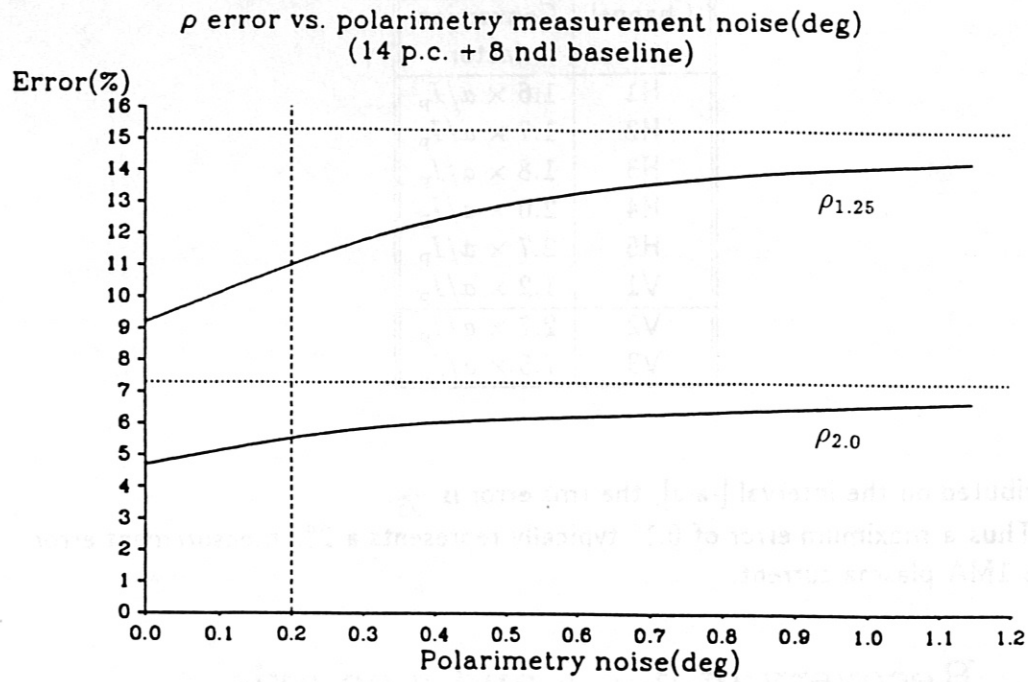

error of $\rho_{1.25}$ and $\rho_{2.0}$ versus error in degrees in $\int n_e \mathbf{B} \cdot \mathbf{dl}$, where the errors are uniformly distributed between $\pm$ the quoted error level.

The recovery shows reasonable robustness — the vertical reference line shows the maximum tolerance of 0.2° in the measurement of rotation angle on a system developed at University College Cork for the RFX experiment in Padua. The horizontal lines mark the recovery error for $\rho_{1.25}$ and $\rho_{2.0}$ with the baseline model consisting of the 14 magnetic measurement p.c.'s only. At 0.2°, most of the gains made by adding the polarimetry measurements are still intact. This seems to indicate that the accuracy required for the diagnostic to significantly improve FP recovery of q is easily attainable when judged against the quoted tolerance of the existing RFX system.

14 Error conversion factors

Although we add absolute errors to the Faraday rotation angles, it is of interest to look at the percentage errors in the signals for a given absolute error in degrees.

Table 5 shows the conversion factor between the two for each channel, where a is the maximum absolute angular error in units of 0.1° and I_p is the plasma current in MA. Note that % error $= \frac{\text{rms error}}{\text{std. dev.}} \times 100$ and for a variable uniformly

Table 5: Percentage error to absolute degrees error conversion factors

Channel	Conversion factor
H1	$1.6 \times a/I_p$
H2	$1.7 \times a/I_p$
H3	$1.8 \times a/I_p$
H4	$2.0 \times a/I_p$
H5	$2.7 \times a/I_p$
V1	$1.2 \times a/I_p$
V2	$2.7 \times a/I_p$
V3	$7.5 \times a/I_p$

distributed on the interval [-a,a], the rms error is $\frac{a}{\sqrt{3}}$.

Thus a maximum error of 0.1° typically represents a 2% measurement error for a 1MA plasma current.

15 Recovery of $\beta_{\rm pol}$, $l_{\rm i}$ and q on axis.

As an additional test we have investigated the improvement in $\beta_{\rm pol}$, $l_{\rm i}$ and $q_{\rm axis}$ recovery using the polarimetry measurements since these parameters are closely linked to the poloidal magnetic field . Table 6 shows summary statistics for the three parameters. The rather wide range of $q_{\rm axis}$ values ($q_{\rm axis,max}/q_{\rm axis,min} = 1.23/.34 = 3.6$) is a consequence of the variation in $l_{\rm i}$ ($l_{\rm i,max}/l_{\rm i,min} = 1.96/.77 = 2.5$) and plasma area (which covered the range $0.9 \leq A \leq 1.5\,{\rm m}^2$, thus ${\rm A_{max}/A_{min}} = 1.5/0.9 = 1.66$). Since the plasma current is fixed at 1 MA, the area determines the average current density: $< j >= 1/{\rm Area}$ (MA m^{-}2) and for a fixed $B_t = 2.5\,{\rm T}$ (and circular flux surfaces) we have $q_{\rm axis} \propto 1/j_{\rm axis}$. As $l_{\rm i}$ is essentially a peaking factor for the current density profile we see that $j_{\rm axis}$ and hence $q_{\rm axis}$ vary with both $< j >$ and $l_{\rm i}$.

Using the same model as in the previous analysis of ρ_ψ, the error versus noise added to the $\int n_e {\rm B} \cdot {\rm dl}$ signals is plotted for $\beta_{\rm pol}$ and $l_{\rm i}$ in fig. 9.

Table 6: Summary statistics for $\beta_{\rm pol}$, $l_{\rm i}$ and $q_{\rm axis}$

Variable	Mean	Std. Dev.	Min	Max
$q_{\rm axis}$	0.78	0.22	0.34	1.23
$l_{\rm i}$	1.28	0.22	0.77	1.96
$\beta_{\rm pol}$	1.14	0.53	0.01	2.19

Figure 9:

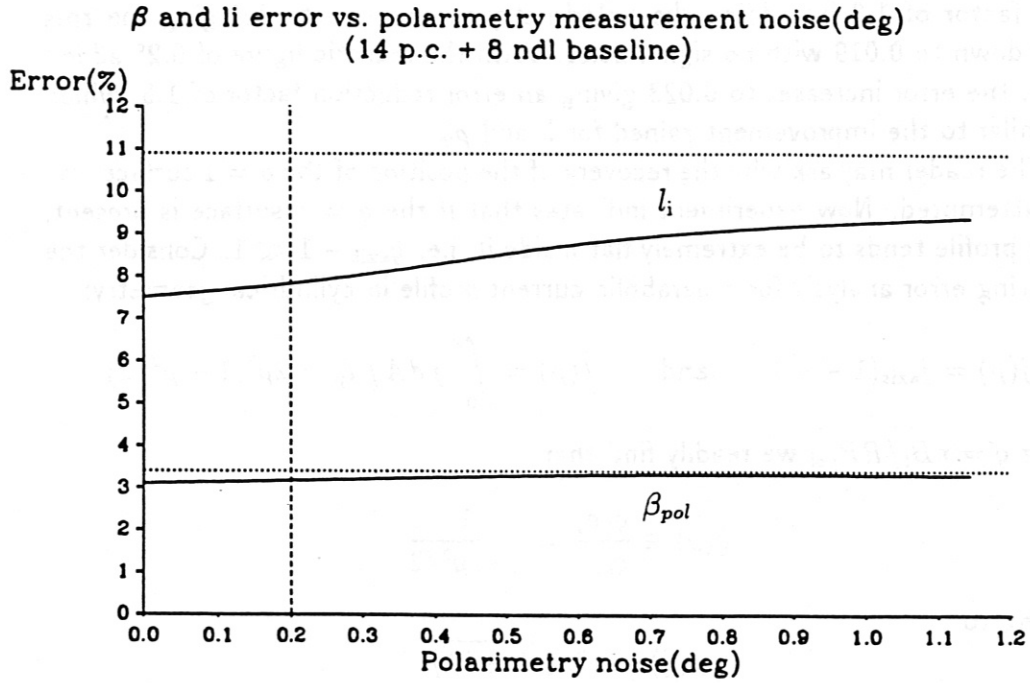

Table 7: Recovery of q_{axis} for various models

Model details (bracket figures = noise levels)	RMSE	Adj. R^2	% error
14 p.c.(1%) + $8\int n_e dl$ (2%)	0.034	0.9763	15.4
14 p.c.(1%) + $8\int n_e dl$ (2%) + $6\int n_e B_{\|\|} dl(0.0°)$	0.019	0.9929	8.4
14 p.c.(1%) + $8\int n_e dl$ (2%) + $6\int n_e B_{\|\|} dl(0.1°)$	0.020	0.9917	9.1
14 p.c.(1%) + $8\int n_e dl$ (2%) + $6\int n_e B_{\|\|} dl(0.2°)$	0.023	0.9896	10.2
14 p.c.(1%) + $8\int n_e dl$ (2%) + $6\int n_e B_{\|\|} dl(0.6°)$	0.029	0.9820	13.4
14 p.c.(1%) + $8\int n_e dl$ (2%) + $6\int n_e B_{\|\|} dl(1.0°)$	0.032	0.9793	14.4

$\beta_{\rm pol}$ shows hardly any improvement, while $l_{\rm i}$ is considerably better determined. These results are consistent with the fact that $\beta_{\rm pol}$ represents the average plasma pressure, and is independent of the current profile, whereas $l_{\rm i}$ is a moment of the current profile, and is hence determined by it.

The results for $q_{\rm axis}$ are presented in table 7. The baseline external magnetic measurements model yields a rmse value of 0.034. This error level is reduced by a factor of 1.8 by adding the polarimetry measurements, bringing the rms error down to 0.019 with no signal noise. With the realistic figure of 0.2° added noise, the error increases to 0.023 giving an error reduction factor of 1.5, which is similar to the improvement gained for $l_{\rm i}$ and ρ_ψ.

The reader may ask why the recovery of the position of the $q = 1$ surface was not attempted. Now experiment indicates that if the $q = 1$ surface is present, the q profile tends to be extremely flat inside it, i.e. $q_{\rm axis} - 1 \ll 1$. Consider the following error analysis for a parabolic current profile in cylindrical geometry:

$$j(\rho) = j_{\rm axis}(1-\rho^2) \qquad \text{and} \qquad \hat{I}(\rho) = \int_0^\rho j\, dA \,/\, I_p = 2\rho^2(1-\rho^2/2)$$

Using $q = rB_t/RB_{pol}$ we readily find that

$$\hat{q}(\rho) \equiv \frac{q(\rho)}{q_{\rm axis}} = \frac{1}{1-\rho^2/2}$$

leading to

$$\rho(\hat{q}) = \sqrt{2}\sqrt{1-1/\hat{q}}$$

Differentiating we find

$$d\,\rho = \frac{d\,\hat{q}}{\sqrt{2}\sqrt{1-1/\hat{q}}\,\hat{q}^2} \qquad \text{or} \qquad \frac{d\,\rho}{\rho} = \frac{d\,\hat{q}}{2\hat{q}(\hat{q}-1)}$$

Thus for $\hat{q} - 1 \ll 1$ the position of the $\hat{q}$ surface becomes indeterminable for finite $d\,\hat{q}$. For the best recovery achieved for $q_{\rm axis}$ above, i.e. rmse ≈ 0.02, this error analysis indicates that for $d\,\rho/\rho \ll 1$ we require $\hat{q} - 1 \gg 0.01$.

16 Minimal p.c. model

So far, the models used in regressions on the database have been very large: 14 p.c.'s and 14 line integrals amount to 435 individual fitting parameters. We now attempt to reduce this model to a minimal size by cutting down the number of magnetic p.c.'s. All eight $\int n_e dl$ measurements must be included because decoupling $B_{||}$ from the $\int n_e \mathbf{B}\cdot\mathbf{dl}$ is aided by all available information on the density profile provided by the eight interferometry signals.

To determine the appropriate minimum number, the rms recovery error of several geometric parameters in the database was examined. Table 8 contains

Table 8: Table of rmse of geometric parameters

# p.c.'s	$b_{\text{ver}}/a_{\text{hor}}$	R_{geo}	Z_{geo}	Z_{top}	R_{in}	R_{out}
7	0.060	20	13	33	16	30
8	0.058	18	11	32	13	29
9	0.051	9	4	17	3	20
10	0.013	1	3	14	3	2
11	0.012	1	3	14	3	2
12	0.010	1	3	13	2	2

Table 9: Recovery of q_{axis} for various models — 10 p.c. baseline

Model details (bracket figures = noise levels)	RMSE	Adj. R^2	% error
10 p.c.(1%) + $8\int n_e dl$ (2%)	0.038	0.9701	17.3
10 p.c.(1%) + $8\int n_e dl$ (2%) + $6\int n_e B_{\|\|} dl(0.0°)$	0.022	0.9900	10.0
10 p.c.(1%) + $8\int n_e dl$ (2%) + $6\int n_e B_{\|\|} dl(0.1°)$	0.023	0.9890	10.5
10 p.c.(1%) + $8\int n_e dl$ (2%) + $6\int n_e B_{\|\|} dl(0.2°)$	0.025	0.9868	11.5
10 p.c.(1%) + $8\int n_e dl$ (2%) + $6\int n_e B_{\|\|} dl(0.6°)$	0.032	0.9796	14.3
10 p.c.(1%) + $8\int n_e dl$ (2%) + $6\int n_e B_{\|\|} dl(1.0°)$	0.034	0.9760	15.5

the relevant figures for these, where $b_{\text{ver}}/a_{\text{hor}}$ is the elongation (dimensionless) and the remainder are in mm.

It appears that a minimum of 10 p.c.'s is required to reproduce the accuracy obtained in [2] using 12 p.c.'s from the standard FP database containing all 4 categories (inner & outer limiter, lower & upper diverter). We now redo the earlier regressions using this reduced model and examine any deterioration in the recovery as a result of narrowing the model. (The results for q_{axis} are again presented as a table.)

For $\rho_{1.25}$ and $\rho_{2.0}$ (fig. 10), the reduced model results in a deterioration in the recovery error by a factor of roughly 1.3; l_i (fig. 11) and q_{axis} (table 9) display similar behaviour while β_{pol} remains practically unaffected. The error reduction factor resulting in adding the line integral signals to the baseline magnetic p.c. model remains more or less the same, (approximately 1.5–1.6), indicating that the more restricted magnetics model does not affect the predictive value of the polarimetry measurements.

Fig. 10

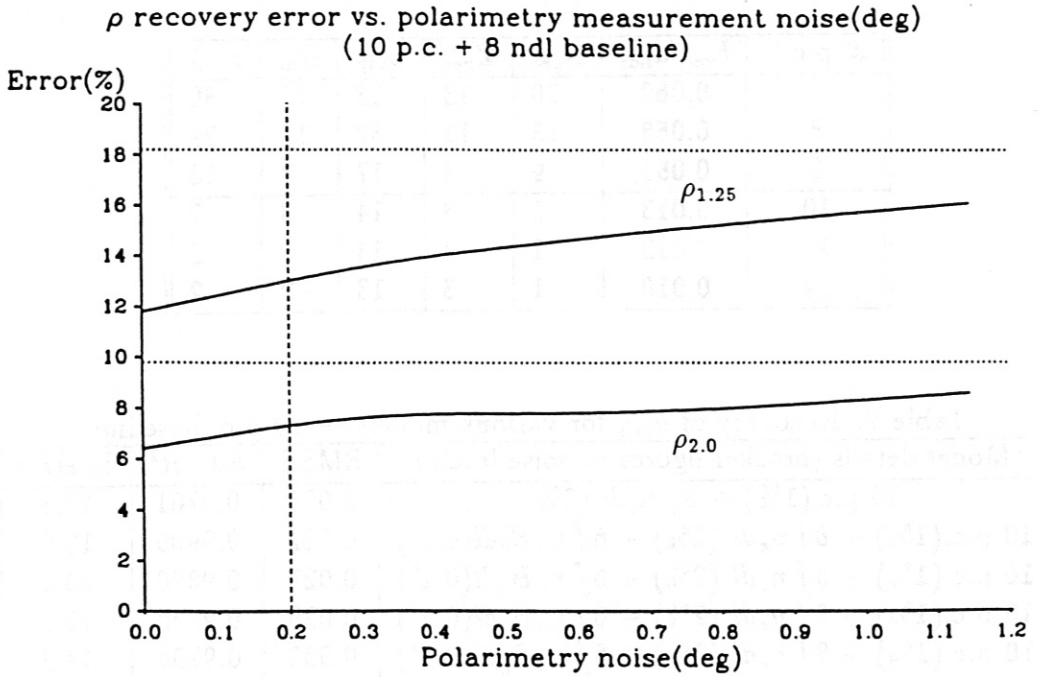
ρ recovery error vs. polarimetry measurement noise(deg)
(10 p.c. + 8 ndl baseline)
Error(%)
20
18
16
14
12
10
8
6
4
2
0
$\rho_{1.25}$
$\rho_{2.0}$
0.0 0.1 0.2 0.3 0.4 0.5 0.6 0.7 0.8 0.9 1.0 1.1 1.2
Polarimetry noise(deg)

Fig. 11

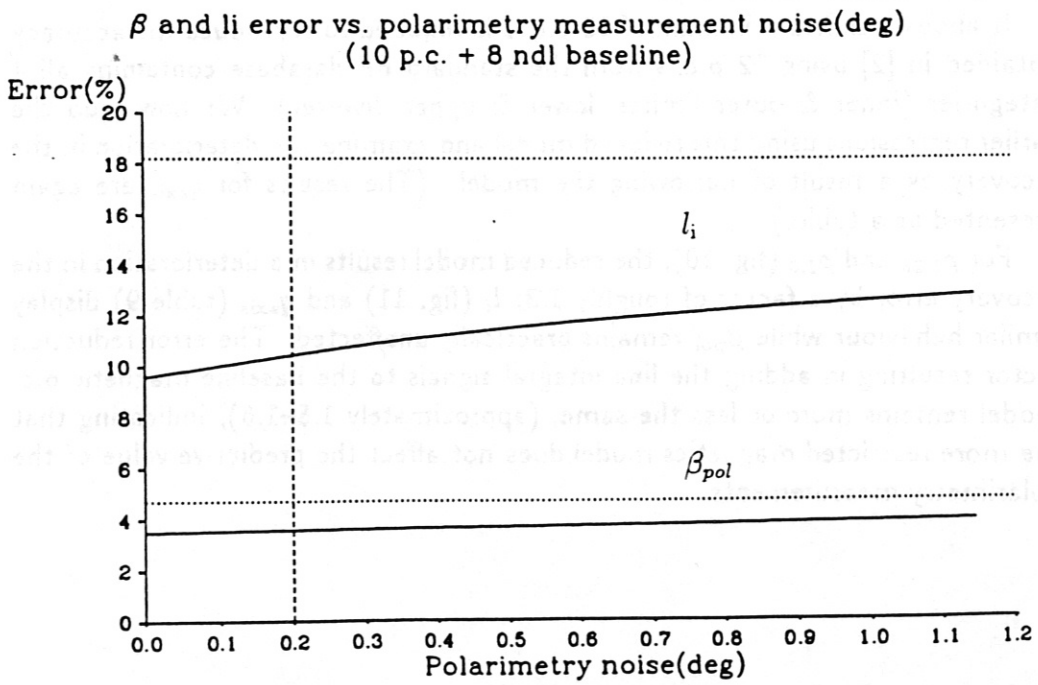
β and li error vs. polarimetry measurement noise(deg)
(10 p.c. + 8 ndl baseline)
Error(%)
20
18
16
14
12
10
8
6
4
2
0
l_i
β_{pol}
0.0 0.1 0.2 0.3 0.4 0.5 0.6 0.7 0.8 0.9 1.0 1.1 1.2
Polarimetry noise(deg)

17 Discussion and Conclusions

The simulated polarimetry measurements strongly reduce the uncertainties in radial position of inner q surfaces (by a factor of ~ 1.6) and the error in l_i in the database. The recovery of the axis q value benefits similarly from the addition of the $\int n_e B_{||} dl$.

The recovery shows reasonable robustness in the presence of signal noise. Based on the quoted maximum tolerance of the system currently in use on RFX ($0.2°$), the angular resolution required to make the diagnostic useful seems to be easily attainable.

The rather accurate determination of the q surfaces, and, in particular, the small error in q_{axis} (rmse ≈ 0.02) must be treated with some caution, since this will be in part due to the restrictions imposed on the current density profiles used in generating the database. In the case of the ASDEX Upgrade equilibrium database (1990-1994) two independent shape parameters were used (see the Database Details section above).

The advantages of using FP for the interpretation of polarimetry data become apparent when we examine the analytic expressions for the evolution of the polarization state when plasma birefringence is considered — they are highly complex, but since they are essentially a known contribution and can be included in the simulated polarimetry measurements, FP can account for the effect with the same procedure as is used here in the case of pure Faraday rotation (the effects of birefringence were not anticipated at the time the database used here was generated).

The regression models used in this work are rather large, containing 435 and 325 terms for the models with 14 and 10 magnetic p.c.'s, respectively. It would be desirable to reduce this furthur, and one promising avenue is the adoption of a neural network approach to this identification problem.

References

[1] De Marco F. & Segre S. E., Plasma Physics 14 245 (1972)

[2] Mc Carthy, P. J., 'An Integrated Data Interpretation System for Tokamak Discharges' Ph.D. thesis, University College Cork, 1992

[3] Lackner K., 'Computation of Ideal MHD equilibria', Comput. Phys. Commun. 12 (1976), 33-44

[4] Mardia K. V., Kent J. T., Bibby J. M., 'Multivariate Analysis', Academic Press, London (1975) pp. 521

[5] Segre S. E., Letter to the editor, Plasma Physics and Controlled Nuclear Fusion, 36 715-718 (1994)

[6] Gehre, O., Private communication, June 10, 1994.